# Laguerre–Gaussian laser filamentation for the control of electric discharges in air

Silin Fu, Leonid Arantchouk, Magali Lozano, André Mysyrowicz, Arnaud Couairon, Aurelien Houard

# Laguerre Gaussian laser filamentation for the control of electric discharges in air

**SILIN FU,[1,2] LEONID ARANTCHOUK,[1] MAGALI LOZANO,[1] ANDRE MYSYROWICZ,[1] ARNAUD COUAIRON,[3] AND AURELIEN HOUARD[1,*]**

[1]*Laboratoire d'Optique Appliquée, ENSTA Paris, CNRS, Ecole polytechnique, IP Paris, 1024 Bd des Maréchaux, 91162 Palaiseau, France*
[2]*School of Nuclear Science and Technology, Lanzhou University, Lanzhou 730000, China*
[3]*Centre de Physique Théorique, CNRS, Ecole polytechnique, IP Paris, route de Saclay, Palaiseau, France*
** aurelien.houard@ensta.fr*

Received XX Month XXXX; revised XX Month, XXXX; accepted XX Month XXXX; posted XX Month XXXX (Doc. ID XXXXX); published XX Month XXXX

**We study the use of Laguerre Gaussian (LG) femtosecond laser filament with multi GW peak power to guide electric sparks in the atmosphere. We demonstrate that LG beam with a vortex phase or with 6 azimuthal phase steps generate a filamentation regime, where a longer and more uniform energy deposition is produced compared to a normal beam with a flat phase. Such filaments can guide electric discharges over much longer distances. This technique could significantly extend the guiding range of laser filaments for lightning control and other long-range atmospheric experiments involving filamentation.**

The ability of intense femtosecond laser pulse to control electric discharge has been extensively studied in the last 20 years [1-9]. While lasers with long energetic pulses have also the ability to guide discharge through the generation of a plasma channel [10] the big advantage of femtosecond pulses is their ability to induce laser filamentation, generating extended plasma strings with moderate input laser energy [11]. The filamentation phenomenon occurs spontaneously during the propagation of a femtosecond laser pulse in air provided its peak power exceeds a critical power $P_{cr}$ of a few GW. Due to the optical Kerr effect, self- focusing of the laser beam produces thin light strings with intensities in the range $10^{13}$-$10^{14}$ W/cm$^2$ called filaments. Through a reduction of the gas density and generation of long-lived charges, the plasma channel created by the filament forms a preferential path for any discharge precursor propagating in air [1-2]. Following the Paschen law, the breakdown voltage reduction in the filament is proportional to the gas density reduction, which directly depends on the density of laser energy deposition. Thus, guiding of meter scale discharge has been reported by many groups using a focused laser filamentation with TW peak power [1-9]. More recently, the guiding of natural lightning over 50 m has even been demonstrated with a kHz Yb:Yag laser of 500 mJ energy per pulse [12-13].

While filamentation spontaneously arises during propagation of a collimated beam, the deposited energy in this collimated filament is relatively weak (a few μJ/cm [14]) and the relative density decrease stays below $10^{-4}$ [15]. Such conditions are not sufficient to guide electric discharges. Typically, a supercritical power ($P >> P_{cr}$) and a slightly focused beam in the so-called lens dominated regime [16] is required to guide a streamer or a leader [1, 17, 18]. In this case intensity clamping is no more effective. Superfilamentation occurs and the extension of the guided zone depends more on the focusing condition than on the laser input energy. To circumvent this limitation and generate a long and uniform guiding filament it has been suggested to use a Bessel like beam [19, 20] or to use multiple pulses focused at different distances [21-23]. These solutions are technically complex, and difficult to scale to hundreds of meters. Recently, the use of Laguerre gauss beam with a vortex phase to produce multiple filaments has been studied in the laboratory [24-28] or numerically [29] and their ability to generate long air waveguides [30-31], to drill a hole in transparent solids [32] or through clouds [33] or to produce vortex lasing emission in nitrogen gas [34-35] has been demonstrated.

In this study we consider three distinct laser modes as input condition for filamentation. The first one is the output mode of the laser, the beam profile of which presents a quasi flat phase. The second one is a vortex beam $LG_{40}$ with topological charge 4, which means that the phase has a variation of 8π along the azimuthal angle. The third one is $LG_{03}$ corresponding to a pie chart with 6 sections, with a π phase shift between each section. Note that in the three cases the beam was apodized by a diaphragm of 22 mm diameter, generating a profile close to a high order super-Gaussian transverse intensity profile also referred as flattened Gaussian beam [36]. Therefore, a more exact denomination of the modes should be "flattened Laguerre-Gauss modes" instead of pure LG modes.

We demonstrate experimentally and numerically that the use of slightly focused LG beams with azimuthal phase shift allows the generation of a longer and more uniform bundle of filaments when compared to a beam with a flat phase. LG are therefore able to guide electric discharges efficiently over longer distances than gaussian beams.

The laser used to produce the filaments is a Ti:Sa CPA laser system

from Amplitude Technology delivering laser pulses at 10 Hz with a central wavelength at 800 nm, a minimum pulse duration of 50 fs and a maximum energy per pulse of 200 mJ. In the experiment the laser beam was limited by a diaphragm with a diameter of 22 mm and it was focused by a converging lens with focal f = 5 m (corresponding to a numerical aperture N.A. = 0.0044). The energy was limited to 22 mJ and the pulse was chirped positively to a duration of 550 fs to avoid damages in the phase plate. This corresponds to a peak power of 31 GW. The LG beams were produced by inserting phase plates in the beam path (fabricated by HOLO-OR) right after the focusing lens. With a pulse duration of 550 fs and a numerical aperture N.A. = 0.0044 we determined experimentally using the method in [37] that the critical power for self-focusing was $P_{cr}(0)$ = 2 GW for the supergaussian laser input beam and $P_{cr}(m = 4)$ = 13 GW for the vortex beam. Experiments were performed at 10 Hz except for the recording of impacts on photosensitive paper that were performed in a single shot regime. The evolution of the beam profile along the z propagation axis and the onset of filament were characterized by inserting photosensitive paper on the beam path [38].The profile of the energy deposition in the filament was also characterized using a microphone to measure the radial pressure wave produced by the filament bundle. Finally, the ability of the different zones of the filamented beam to decrease the breakdown voltage or to guide electric discharge was characterized by producing centimeter scale discharges using a DC voltage [2] and by producing decimeter scale discharges with a Tesla voltage generator (see description in [39]).

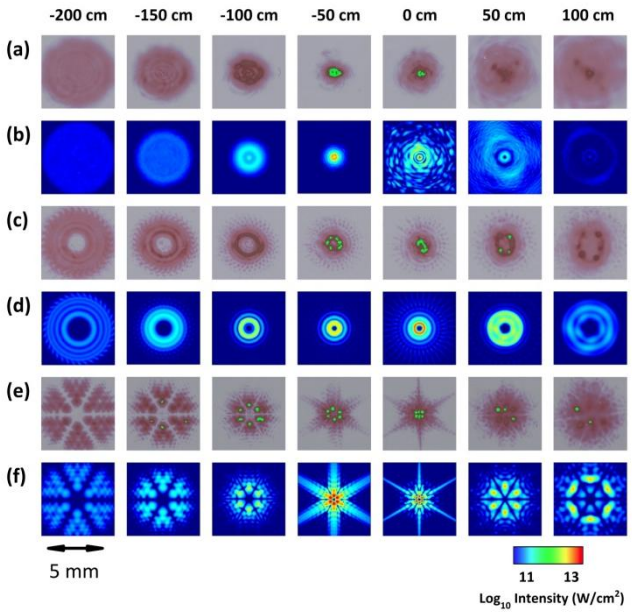


**Fig. 1.** Beam profile measured along propagation axis z on photosensitive paper for a supergaussian beam $LG_{00}$ (a), a vortex beam $LG_{40}$ (c) and a 6-sectors beam $LG_{03}$ (e). The corresponding intensity profiles obtained from numerical simulations are respectively shown in subfigure (b), (d) and (f). The laser pulse propagates from left to right and position z = 0 corresponds to the geometrical focus of the beam.

First, the effect of the vortex and the 6Q phase on the filamentation process has been investigated using impact of single shot laser pulse on photosensitive paper. Fig. 1 presents the evolution of the beam profile along the propagation axis z [30]. The pink color corresponds to moderate laser intensity, while the green color indicates the burned area of the paper, where the estimated laser intensity exceeds the threshold for ionization of air. Note that the response of the paper is not linear with the laser intensity.

In the case of the supergaussian beam (Fig. 1(a)) filamentation appears about 1 meter before the focus, then a dense bundle of fused filament is observed over 1 meter. This seems to corresponds to the superfilamentation regime where the fusion of multiple filaments creates a filament with intensity higher than the clamping intensity [38, 40]. After the focus, only a weak classical filament is observed on the axis over one meter.

In the case of the vortex the filaments appear a bit later than for the 6-sector beam at z = -50 cm. About 6 filaments are visible at -100 cm, forming a quasi continuous ring of plasma at the focus. Then this ring diverges and only 3 filaments remain 50 cm after the focus.

In the case of the 6-sector beam, on can see first strong diffraction effects during the linear propagation of the beam. The beam pattern observed at z = - 200 cm results from the diffraction of the beam by the edge of the sectors on the waveplate and by the circular aperture of the diaphragm. At z = - 150 cm the first filaments appear at the intensity maxima created by the diffraction pattern. Then between -100 cm and 50 cm one can distinguish 6 filaments perfectly aligned on a ring, the diameter of which varies between 1.9 mm (at the beginning) and 0.7 mm (at the geometric focus). Note that the size of the filament ring generated by the m4 vortex is very close to the size of the ring of filament produced by the 6-sector beam (Fig 1(c) and 1(c)).

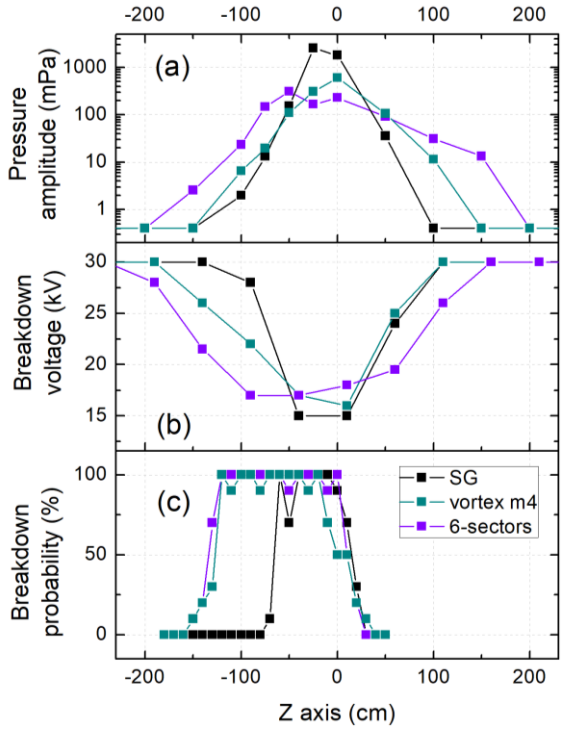


**Fig. 2.** (a) Amplitude of the lateral pressure wave recorded by a microphone as a function of the position z along the laser axis for the three laser modes considered. (b) Threshold for breakdown DC voltage between two plane electrodes separated by 10 mm measured along propagation axis z for the 3 laser modes. (c) Breakdown probability between two pointed electrodes separated by 30 cm and connected to the Tesla generator measured as function of the position of the electrodes. Here, z corresponds to the position of the first electrode, while the second electrode is 30 cm after (z + 30).

Then the energy deposition produced by the filament along z axis has been characterized using transverse acoustic measurement. Indeed, the amplitude of the radial pressure wave produced by the filament is proportional to the density of deposited energy in the filament [41]. A broadband microphone (GRAS Model 46BH 1/4") placed 3 cm away from the beam center has been displaced along z to measure the amplitude of the radial pressure wave emitted by the filament (see [17] for description). The result is presented in Fig. 2(a) for the three beams considered. For the supergaussian beam, one can see that the energy deposition is maximum 20 cm before the focus and that the width (FWHM) of the heated zone is about 150 cm. The vortex case (blue curve) presents a maximum at the focus and a width of 200 cm. Finally, the 6-sectors beam (violet curve) produces a maximum at z = -50 cm and extends over ~250 cm. These results are in good agreement with the burn patterns presented in Fig. 1. The total deposited energy was respectively of 3.8 mJ for the supergaussian beam, 2.2 mJ for the 6 sectors beam and 1.8 mJ for the vortex.

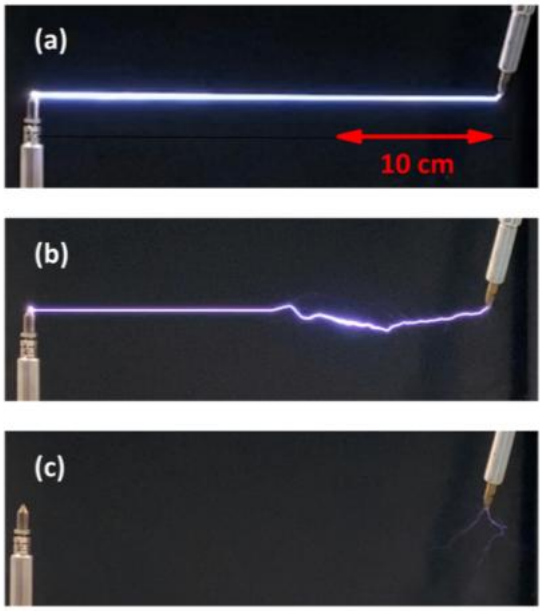


**Fig. 3**. Still image of a fully laser guided discharge (a), a partially guided discharge (b) and an event where no spark occurred (c). The distance between the electrodes is 30 cm and the laser energy was 22 mJ.

We then measured the local decrease of breakdown voltage along z produced by the LG filaments using a spark gap. The spark gap was made of two circular disks of copper pierced in the center and separated by 10 mm. The hole in the center had a diameter of 3 mm and the diameter of the disk was 2 cm. The disks were directly connected to a DC High Voltage power supply (Brandenburg 2807 Alpha Serial II). In the absence of laser, the measured voltage breakdown was 30 kV. The breakdown voltage in the presence of the filament has been measured along z by displacing the electrodes along the laser axis. In the absence of laser filament the breakdown voltage threshold in the gap is 30 kV. This value of 30 kV/cm corresponds exactly to the natural breakdown field in dry air at 1 bar for a uniform DC electric field [42]. In the presence of the filament, a decrease of the breakdown electric field up to 50% is observed around the geometrical focus. We note that the shape of the decrease of the breakdown field induced by the three type of filament presented in Fig. 2(b) is very similar to the shape of the acoustic measurement presented in Fig. 2(a). Again, the vortex and the 6-sectors modes produce a longer guiding zone than the SG mode and the longest guiding length is obtained with the 6-sectors beam.

Finally, we tested the guiding efficiency of the three beams over decimeter scale discharges with a pulsed Tesla generator delivering voltage pulses of 315 kV. The breakdown probability between two pointed electrodes separated by 30 cm and connected to the Tesla generator was measured as function of the position of the electrodes. The result is presented in Fig. 2(c), where z corresponds to the position of the first electrode, while the second electrode is 30 cm after (z + 30). In absence of laser, we observe no discharge between the electrodes (see Fig. 3c). The breakdown probability is calculated over 10 shots. When the breakdown occurs, we observe either a partial or a full guiding of the discharge (as illustrated in Fig. 3a and b). With the SG beam, a breakdown probability of 100 % is obtained between z = -70 cm and z = 10 cm. This length is twice longer with the LG beams, where it starts at -130 cm. We note that the curves obtained in Fig. 2(c) do not match perfectly with the ones in Figure 2(a) and (b). We explain this, first, by the fact that the Tesla gap length is much larger than the sampling resolution of the two other diagnostics used, and second, by the strong non-uniformity of the electric field in the 40 cm gap that produced asymmetric discharge precursors (as seen in Fig. 3(c)).

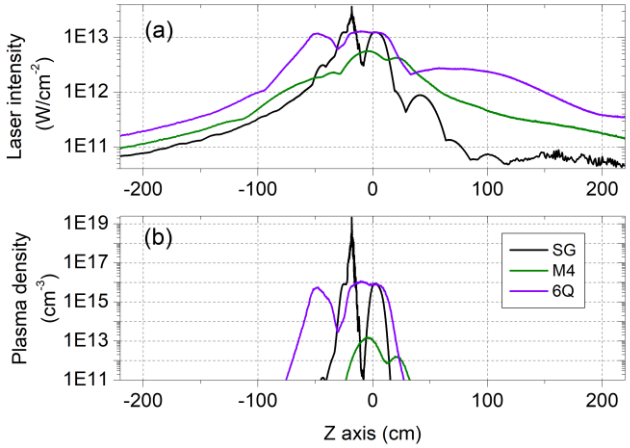


**Fig. 4**. Calculated laser maximum intensity (a), plasma density (b) as a function of the propagation distance z for the three considered laser modes.

To compare the filamentation mechanism in the different cases, numerical simulations were performed to model the nonlinear propagation of the laser pulse. As in earlier works reporting simulations of multiple filamentation [38, 43, 44], the electric field envelope satisfies a nonlinear Schrödinger equation used in the limit of frozen time approximation, which is justified in the case of laser pulses with a duration of 550 fs propagation over a short distance compared to the dispersion length. The model includes the effects of diffraction, the optical Kerr effect with nonlinear refractive index coefficient $n_2$ =2.9 x $10^{-19}$ cm$^2$/W, plasma induced effects including plasma defocusing, plasma absorption and nonlinear losses due to multiphoton ionization with cross section $\sigma_8 = 3.7 \times 10^{-96} s^{-1}$ $cm^{16}.W^{-8}$. Ionization induced effects are implemented by a preliminary mapping between peak intensity and electron density through the ionization model using a

fixed Gaussian pulse profile over the whole propagation length. The numerical scheme for space marching the laser pulse relies on standard techniques, described in [45], propagating the spectral angular components of the field envelope for linear effects and field spatial components in direct space for nonlinear effects. To start from realistic input conditions, the initial laser beam in the simulations is a 1 cm large super-Gaussian beam of order 16, which represents the experimental beam immediately after the focusing lens and thus carries a parabolic phase describing the effect of the lens, a phase increment describing the effect of the 6-sectors or M4 phase plate, and additional white noise describing irregularities of the beam profile.

The results are presented in Fig. 4, where the laser maximum intensity and plasma density are plotted as a function of the propagation distance *z*. Note that the calculated plasma density observed for the vortex beam is relatively low compared to classical filament, with a density between $10^{11}$ and $10^{13}$ $cm^{-3}$, while the 6-sectors filament exhibit classical features of femtosecond filamentation, such as the saturation of the laser intensity at $10^{13}$ $W/cm^2$ and a peak plasma density around $10^{16}$ $cm^{-3}$. In the case of the supergaussian beam we retrieve an intensity profile corresponding to a superfilamentation regime around the geometrical focus, in agreement with the acoustic measurement presented in Fig. 2(a). These results show a qualitative agreement with the acoustic measurements presented in Fig. 2.

We have demonstrated that the use of LG beams with azimuthal phase shift allows the generation of a longer and more uniform bundle of filaments when compared to a laser beam with a flat phase. LG are therefore able to guide electric discharges efficiently over longer distances than gaussian beams.

For application such as the guiding of long electric discharges [1], remote LIBS [46] water condensation [47], or cloud clearing [48], it is required to have locally a sufficient density of deposited energy (need for focusing) and at the same time, a long and uniform effect. We believe that the use of LG is a promising solution to generate the desired long and uniform plasma filaments for these applications. In addition, the stability of the beam phase profile of LG beams with respect to local turbulence has been demonstrated is several studies, making them particularly suitable for long range propagation in the atmosphere [49-52].

**Acknowledgments.** The authors acknowledge the support of Y.-B. André and financial support from Chinese Scholarship Council for SF.

**Disclosures.** The authors declare no conflicts of interest.

**Data availability.** Data underlying the results presented in this paper are not publicly available at this time but may be obtained from the authors upon reasonable request.

## REFERENCES

1. D. Comtois, et al., Appl. Phys. Lett. **76**, 819–821 (2000).
2. S. Tzortzakis, et al., Phys. Rev. E **64**, 057401 (2001).
3. P. Rambo, J. Schwarz and J.-C. Diels, J. Opt. A: Pure Appl. Opt. **3** 146 (2001).
4. M. Rodriguez, et al., Opt. Lett. **27**, 772 (2002).
5. T. Fujii, et al., Phys. Plasmas **15**, 013107 (2008).
6. A. A. Ionin, et al., Appl. Phys. Lett. **100**, 104105 (2012).
7. F. Théberge, J.-F. Daigle, J.-C. Kieffer, F. Vidal, and M. Châteauneuf, Scientific reports **7**, 1–8 (2017).
8. A. Schmitt-Sody, J. Elle, A. Lucero, M. Domonkos, A. Ting, and et V. Hasson, AIP Adv. **7**, 035018 (2017).
9. Z. Pei, et al., Physics of Plasmas, **30**, 043511 (2023).
10. S. Uchida, et al., J. Opt. Technol. **66**, 199–202 (1999).
11. A. Couairon, A. Mysyrowicz, Phys. Rep. **441**, 47-189 (2007)
12. A. Houard, et al., Nat. Photonics **17**, 231 (2023).
13. P. Walch et al., Sci. Rep. **13**, 18542 (2023).
14. E. W. Rosenthal, et al., Optics Letters **41**, 3908 (2016).
15. J. K. Wahlstrand, et al., Optics Letters **39**, 1290 (2014).
16. K. Lim, M. Durand, M. Baudelet, and M. Richardson, Sci. Rep. **4**, 7217 (2014).
17. G. Point, E. Thouin, A. Mysyrowicz and A. Houard, Optics Express **24**, 6271 (2016).
18. B. Forestier, et al., AIP Advances **2**, 012151 (2012).
19. M. Clerici et al., Sci. Adv. **1**, e1400111 (2015).
20. M. Scheller, N. Born, W. Cheng, and P. Polynkin, Optica **1**, 125-128 (2014).
21. P. Polynkin, Appl. Phys. Lett. **16,** 161102 (2017).
22. J. Papeer, et al., Sci Rep **9**, 407 (2019).
23. P. J. Skrodzki, T. Nutting, M. Burger, L. A. Finney, J. Nees, and I. Jovanovic, in CLEO 2023, Technical Digest Series (Optica Publishing Group, 2023), paper ATh4I.4.
24. P. Polynkin, C. Ament, and J.V. Moloney, Phys. Rev. Lett. **111**, 023901 (2013).
25. M. Burger, P. Polynkin, and I. Jovanovic, Opt. Express **28**, 36812-36821 (2020).
26. N. Barbieri, et al., Appl. Phys. Lett. **104**, 261109 (2014).
27. L. Liu et al., J. Phys. B: At. Mol. Opt. Phys. **44** 215404 (2011).
28. H. Gao, W. Chu, G. Yu, B. Zeng, J. Zhao, Z. Wang, W. Liu, Y. Cheng, and Z. Xu, Opt. Express **21**, 4612-4622 (2013).
29. L. Xu, D. Li, J. Chang, T. Xi, Z. Hao, Results in Physics **26**, 104334 (2021).
30. S. Fu, B. Mahieu, A. Mysyrowicz, A. Houard, Optics Letters **47**, 5228 (2022).
31. A. Goffin, A. Tartaro, and H. M. Milchberg, Optica **10**, 505-506 (2023).
32. C. Xie,V. Jukna, C. Milián, et al. , Sci. Rep. **5**, 8914 (2015).
33. T. Wang, S. Bin Ali Reza, F. Buldt, P. Bassène, M. N'Gom, J. Appl. Phys. **133**, 043102 (2023).
34. Y. Hu, et al., Optica **10**, 682-687 (2023).
35. J. Gao, X. Zhang, Y. Wang, et al., Commun. Phys. **6**, 97 (2023).
36. M. Santarsiero and R. Borghi, J. Opt. Soc. Am. A **16**, 188-190 (1999).
37. W. Liang, et al. Opt. Express **31**, 1557-1566 (2023).
38. G. Point, Y. Brelet, A. Houard, V. Jukna, C. Milián, J. Carbonnel, Y. Liu, A. Couairon, and A. Mysyrowicz, Phys. Rev. Lett. **112**, 223902 (2014).
39. P. Walch, et al., Physics of Plasmas **30**, 083503 (2023).
40. D Pushkarev et al., New J. Phys. **21** 033027 (2019).
41. G. Point, C. Milián, A. Couairon, A. Mysyrowicz, and A. Houard, Journal of Physics B **48**, 094009 (2015).
42. Y. P. Raizer, Gas Discharge Physics (Berlin: Springer) (1991).
43. C. Milián *et al.,* J. Phys. B: At. Mol. Opt. Phys. **48** 094013 (2015).
44. I. Dicaire, V. Jukna, C. Praz, C. Milian, L. Summerer, A. Couairon, Laser Photonics Reviews **10**, 481-93 (2016).
45. A. Couairon, et al., The European Physical Journal Special Topics **199**, 5-76 (2011).
46. K. Stelmaszczyk, et al., Appl. Phys. Lett. **85**, 3977–3979 (2004).
47. V. Shumakova, et al., Optica **8**, 1256-1261 (2021).
48. G. Schimmel, et al., Optica **5**, 1338–1341 (2018).
49. W. Cheng, J. W. Haus, and Q. Zhan, Opt. Express **17**, 17829-17836 (2009).
50. A. Goffin, et al., Phys. Rev. X **13**, 011006 (2023).
51. B. Yan et al., Opt. Laser Technol. **164**, 109515 (2023).
52. D. Zhu at al., Sensors 23, 1772 (2023).

## References


1. D. Comtois, C. Y. Chien, A. Desparois, F. Génin, G. Jarry, T. W. Johnston, J.-C. Kieffer, B. L. Fontaine, F. Martin, R. Mawassi, H. Pépin, F. A. M. Rizk, and F. Vidal, "Triggering and guiding leader discharges using a plasma channel created by an ultrashort laser pulse," Appl. Phys. Lett. **76**, 819–821 (2000).
2. S. Tzortzakis, B. Prade, M. Franco, A. Mysyrowicz, S. Hüller, et P. Mora, Femtosecond laser-guided electric discharge in air, Phys. Rev. E **64**, 057401 (2001) doi: 10.1103/PhysRevE.64.057401
3. P. Rambo, J. Schwarz and J.-C. Diels, High-voltage electrical discharges induced by an ultrashort-pulse UV laser system, J. Opt. A: Pure Appl. Opt. **3** 146–158 (2001)
4. M. Rodriguez, et al. "Triggering and guiding megavolt discharges by use of laser-induced ionized filaments," Opt. Lett. **27**, 772 (2002).
5. T. Fujii, M. Miki, N.Goto, A. Zhidkov, T. Fukuchi, Y. Oishi, and K. Nemoto, "Leader effects on femtosecond-laser-filament-triggered dis- charges," Phys. Plasmas **15**, 013107 (2008).
6. A. A. Ionin, S. I. Kudryashov, A. O. Levchenko, L. V. Seleznev, A. V. Shutov, D. V. Sinitsyn, I. V. Smetanin, N. N. Ustinovsky, V. D. Zvorykin, "Triggering and guiding electric discharge by a train of ultraviolet picosecond pulses combined with a long ultraviolet pulse," Appl. Phys. Lett. **100**, 104105 (2012)
7. F. Théberge, J.-F. Daigle, J.-C. Kieffer, F. Vidal, and M. Châteauneuf, "Laser-guided energetic discharges over large air gaps by electric-field enhanced plasma filaments," Scientific reports **7**, 1–8 (2017)
8. A. Schmitt-Sody, J. Elle, A. Lucero, M. Domonkos, A. Ting, and et V. Hasson, "Dependence of single-shot pulse durations on near-infrared filamentation-guided breakdown in air," AIP Adv. **7**, 035018 (2017)
9. Z. Pei, W. Chen, X. Fan, J. Gu, S. Huang, X. Liu, Z. Fu, B. Du, T. Wang, R. Zhang, Q. Zhang, "The contribution of femtosecond laser filaments to positive and negative breakdown discharge in a long air gap," Physics of Plasmas, **30**, 043511 (2023) https://doi.org/10.1063/5.0138646
10. S. Uchida, et al. Laser-triggered lightning in field experiments. J. Opt. Technol. **66**, 199–202 (1999).
11. A. Couairon, A. Mysyrowicz, "Femtosecond filamentation in transparent media," Phys. Rep. **441**, 47-189 (2007)
12. A. Houard, P. Walch, T. Produit, et al., "Laser-guided lightning," Nat. Photonics **17**, 231 (2023).
13. P. Walch et al., Long distance laser filamentation using Yb:YAG kHz laser, Sci. Rep. **13**, 18542 (2023).
14. E. W. Rosenthal, N. Jhajj, I. Larkin, S. Zahedpour, J. K. Wahlstrand, and H. M. Milchberg, "Energy deposition of single femtosecond filaments in the atmosphere," Optics Letters **41**, 3908 (2016).
15. J. K. Wahlstrand, N. Jhajj, E. W. Rosenthal, S. Zahedpour, and H.M. Milchberg, "Direct Measurement of the Acoustic Waves Generated by Femtosecond Filaments in Air," Optics Letters **39**, 1290 (2014).
16. K. Lim, M. Durand, M. Baudelet, and M. Richardson, "Transition from linear- to nonlinear-focusing regime in filamentation," Sci. Rep. **4**, 7217 (2014).
17. G. Point, E. Thouin, A. Mysyrowicz and A. Houard, "Energy deposition from focused terawatt laser pulses in air undergoing multifilamentation," Optics Express **24**, 6271 (2016).
18. B. Forestier, A. Houard, I. Revel, M. Durand, Y. B. André, B. Prade, A. Jarnac, J. Carbonnel, M. Le Nevé, J. C. de Miscault, B. Esmiller, D. Chapuis, and A. Mysyrowicz, Triggering, guiding and deviation of long air spark discharges with femtosecond laser filament, AIP Advances **2**, 012151 (2012).
19. M. Clerici et al., Laser-assisted guiding of electric discharges around objects. Sci. Adv. **1**, e1400111 (2015). DOI:10.1126/sciadv.1400111
20. M. Scheller, N. Born, W. Cheng, and P. Polynkin, "Channeling the electrical breakdown of air by optically heated plasma filaments," Optica **1**, 125-128 (2014)
21. P. Polynkin; Multi-pulse scheme for laser-guided electrical breakdown of air. Appl. Phys. Lett. **16,** 161102 (2017) https://doi.org/10.1063/1.4985265
22. J. Papeer, et al. "Towards Remote Lightning Manipulation by Meters-long Plasma Channels Generated by Ultra-Short-Pulse High-Intensity Lasers," Sci Rep **9**, 407 (2019). https://doi.org/10.1038/s41598-018-36643-2
23. P. J. Skrodzki, T. Nutting, M. Burger, L. A. Finney, J. Nees, and I. Jovanovic, "Guiding of Spectroscopic Signal with a Concatenated Filament-Driven Waveguide," in CLEO 2023, Technical Digest Series (Optica Publishing Group, 2023), paper ATh4I.4.
24. P. Polynkin, C. Ament, and J.V. Moloney, "Self-Focusing of Ultraintense Femtosecond Optical Vortices in Air," Phys. Rev. Lett. **111**, 023901 (2013).
25. M. Burger, P. Polynkin, and I. Jovanovic, "Filament-induced breakdown spectroscopy with structured beams," Opt. Express **28**, 36812-36821 (2020).
26. N. Barbieri, Z. Hosseinimakarem, K. Lim, M. Durand, M. Baudelet, E. Johnson, M. Richardson, "Helical filaments," Appl. Phys. Lett. **104**, 261109 (2014).
27. L. Liu et al., "Fine control of multiple femtosecond filamentation using a combination of phase plates," J. Phys. B: At. Mol. Opt. Phys. **44** 215404 (2011).
28. H. Gao, W. Chu, G. Yu, B. Zeng, J. Zhao, Z. Wang, W. Liu, Y. Cheng, and Z. Xu, "Femtosecond laser filament array generated with step phase plate in air," Opt. Express **21**, 4612-4622 (2013).
29. L. Xu, D. Li, J. Chang, T. Xi, Z. Hao, "Helical filaments array generated by femtosecond vortex beams with lens array in air," Results in Physics **26**, 104334 (2021).
30. S. Fu, B. Mahieu, A. Mysyrowicz, A. Houard, Femtosecond filamentation of optical vortices for the generation of optical air waveguides, Optics Letters **47**, 5228 (2022).
31. A. Goffin, A. Tartaro, and H. M. Milchberg, "Quasi-steady-state air waveguide," Optica **10**, 505-506 (2023).
32. C. Xie,V. Jukna, C. Milián, et al. , "Tubular filamentation for laser material processing," Sci. Rep. **5**, 8914 (2015). https://doi.org/10.1038/srep08914
33. T. Wang, S. Bin Ali Reza, F. Buldt, P. Bassène, M. N'Gom, "Structured light signal transmission through clouds," J. Appl. Phys. **133**, 043102 (2023) https://doi.org/10.1063/5.0129902
34. Y. Hu, Z. Ye, H. Li, C. Lu, F. Chen, J. Wang, S. Pan, M. Zhang, J. Gao, and J. Wu, "Generation of vortex N2+ lasing," Optica **10**, 682-687 (2023).
35. J. Gao, X. Zhang, Y. Wang, et al. « Structured air lasing of $N_2^+$," Commun. Phys. **6**, 97 (2023). https://doi.org/10.1038/s42005-023-01226-9
36. M. Santarsiero and R. Borghi, "Correspondence between super-Gaussian and flattened Gaussian beams," J. Opt. Soc. Am. A **16**, 188-190 (1999)
37. W. Liang, et al. Experimentally determined critical power for self-focusing of femtosecond vortex beams in air by a fluorescence measurement, Opt. Express **31**, 1557-1566 (2023). https://doi.org/10.1364/OE.474355
38. G. Point, Y. Brelet, A. Houard, V. Jukna, C. Milián, J. Carbonnel, Y. Liu, A. Couairon, and A. Mysyrowicz, Superfilamentation in Air, Phys. Rev. Lett. **112**, 223902 (2014)
39. P. Walch, L. Arantchouk, B. Mahieu, M. Lozano, Y.-B. André, A. Mysyrowicz, A. Houard,Study of consecutive long-lived meter-scale laser-guided sparks in air, Physics of Plasmas **30**, 083503 (2023)
40. D Pushkarev et al., Transverse structure and energy deposition by a subTW femtosecond laser in air: from single filament to superfilament, New J. Phys. **21** 033027 (2019).
41. G. Point, C. Milián, A. Couairon, A. Mysyrowicz, and A. Houard, Generation of long-lived underdense channels using femtosecond filamentation in air, Journal of Physics B **48**, 094009 (2015).
42. Y. P. Raizer, Gas Discharge Physics (Berlin: Springer) (1991)

43. C. Milián *et al.,* "Laser beam self-symmetrization in air in the multifilamentation regime," *J. Phys. B: At. Mol. Opt. Phys.* **48** 094013 (2015)
44. I. Dicaire, V. Jukna, C. Praz, C. Milian, L. Summerer, A. Couairon, "Spaceborne laser filamentation for atmospheric remote sensing," Laser Photonics Reviews **10**, 481-93 (2016).
45. A. Couairon, E. Brambilla, T. Corti, D. Majus, O. de J. Ramírez-Góngora, M. Kolesik, "Practitioner's guide to laser pulse propagation models and simulation: Numerical implementation and practical usage of modern pulse propagation models," The European Physical Journal Special Topics **199**, 5-76 (2011).
46. K. Stelmaszczyk, P. Rohwetter, G. Méjean, J. Yu, E. Salmon, J. Kasparian, R. Ackermann, J.-P. Wolf, L. Wöste, Long-distance remote laser-induced breakdown spectroscopy using filamentation in air. Appl. Phys. Lett. **85**, 3977–3979 (2004) https://doi.org/10.1063/1.1812843
47. V. Shumakova, E. Schubert, T. Balčiūnas, M. Matthews, S. Ališauskas, D. Mongin, A. Pugžlys, J. Kasparian, A. Baltuška, and J.-P. Wolf, "Laser induced aerosol formation mediated by resonant excitation of volatile organic compounds," Optica **8**, 1256-1261 (2021)
48. G. Schimmel, et al. Free space laser telecommunication through fog, Optica **5**, 1338–1341 (2018) doi: 10.1364/OPTICA.5.001338
49. W. Cheng, J. W. Haus, and Q. Zhan, "Propagation of vector vortex beams through a turbulent atmosphere," Opt. Express **17**, 17829-17836 (2009)
50. A. Goffin, et al., Optical Guiding in 50-Meter-Scale Air Waveguides, Phys. Rev. X **13**, 011006 (2023). https://doi.org/10.1103/PhysRevX.13.011006
51. B. Yan et al., Filamentation of femtosecond vortex laser pulses in turbulent air, Opt. Laser Technol. **164**, 109515 (2023). https://doi.org/10.1016/j.optlastec.2023.109515
52. D. Zhu at al., The effect of air turbulence on Vortex Beams in nonlinear propagation, Sensors 23, 1772 (2023). https://doi.org/10.3390/s23041772